Statistical Mechanics of Ionomeric Colloids. 2. Ionomer Conformational Equilibria

David Ronis

Department of Chemistry, McGill University, 801 Sherbrooke Street West, Montreal, Quebec, Canada H3A 2K6

Received September 9, 1992; Revised Manuscript Received December 3, 1992

ABSTRACT: Conformational equilibria in the charged region of spherical ionomeric colloids are studied using a self-consistent mean-field Monte Carlo method. It is shown that the ionomers do not adopt a single type of conformation but instead exhibit both rodlike and swollen coillike regions. The extent of these regions can be controlled by varying the screening length, curvature of the colloid core, and aggregation number.

I. Introduction

Dilute suspensions of highly charged colloidal particles exhibit many interesting phenomena and have provided a wealth of experimental data with which to test theory. For example, in equilibrium, these systems exhibit strong liquidlike correlations and can form crystalline phases, even at ultralow packing fractions if the electrostatic screening is poor,[1] and can be viewed as extremely asymmetric electrolyte solutions.

Good fits to experimental scattering data can be obtained using modern liquid-state theories which treat the suspension as a single component (the colloid) interacting through an effective potential, specifically, a screened-Coulomb potential, as suggested by the Debye–Hückel calculations of Verwey and Overbeek.[2] On the other hand, accurate, numerically practical theories which include the counterions explicitly have only been developed recently.[3] One advantage of these latter approaches is that the average counterion distributions around the colloidal particles can be calculated, and these can be compared with recent X-ray scattering experiments.[4]

Recently, block-copolymer micelles have been fabricated.[5] One of the diblocks is ionomeric while the other is not, and depending on the choice solvent, micelles (with the charge on the outside) or reverse micelles can be formed. While these systems have many features in common with the simpler charged colloids, several important differences exist. For example, since the charge is distributed in an ionomeric layer, a much higher net charge per aggregate is possible. The theory developed in ref 6 can treat interaggregate static correlations and the underlying counterion charge distributions, provided that the ionomer charge in the ionomeric layer is approximated as a spherically symmetric continuum with any assumed charge distribution.

In reality, however, the ionomeric layer is comprised of flexible chains and the question of conformational equilibrium must be examined. This is an old question, perhaps first arising within the context of charged polyelectrolytes.[7] In these systems, while mean-field approaches are quite possible,[8] a fully molecular approach (e.g., via Monte Carlo simulation) is a formidable task even for simple models of long charged chains.[9] The problem is further complicated for colloidal particles, since the density of ionomers is not necessarily small, and thus inter- as well as intrachain interactions must be considered.

Neutral chains attached to surfaces have received much attention over the years. For example, continuum models of random polymers, with[10-12] and without[13] phenomenological excluded-volume interactions, have been used to calculate the monomer density for neutral chains. Examples of other approaches are scaling theories[14] and the self-consistent mean-field free energy density constructed by Ball et al.[15] Finally, Murat and Grest[16] have performed molecular dynamics simulations on chains attached to cylindrical or spherical surfaces.

In ref 6, the electrostatic contributions to the system's free energy were computed for *assumed* ionomer average densities (in particular, for rodlike and dense-coil distributions). This approach can be used to determine the most stable configuration only under the additional assumption that the electrostatic contributions are dominant and provided that the configurations explicitly considered are the correct ones.

In this work, the conformational equilibria in the ionomeric region of block-copolymer micellar colloids will be examined using a combination of mean-field approximations and Monte Carlo methods. In the next section, a mean-field theory for a single ionomeric polymer attached to a spherical surface is constructed. For this work, electrostatic interactions will be included via an effective potential calculated within the linearized Debye–Hückel approximation and excluded-volume interactions will be described by a Flory-like excluded-volume energy. Both of these contributions can be written as simple functionals of the average monomer density.

Having incorporated all interionomer interactions in a mean field, all that remains is to treat a single chain near a surface in some arbitrary external field (which must then be determined self-consistently). This part of the calculation is numerically feasible in the continuum limit, and several aspects of single chains in external fields are discussed in the appendix. It is easy to show that the continuum results presented here generalize those of refs 11–13.

Rather than solve the continuum-limit equations, a self-consistent Monte Carlo method is presented in section III. In short, the configurations of a single chain in an external field are sampled using a traditional Monte Carlo scheme, with the external potential being updated after some number of Monte Carlo steps. The entire procedure is repeated until self-consistency is obtained.

Section IV contains results for systems with different aggregation numbers, screening lengths, and excluded-volume parameters. Two aspects of the results are worth mentioning here. First, continuum approximations, while excellent for neutral chains, are inadequate for poorly screened charged chains. Second, a simple single morphological description of the ionomeric region (e.g., rod or coil) is not correct. The ionomers will exhibit both rodlike and coillike behavior at different distances from the colloid core, where the extent of each type of behavior depends

0024-9297/93/2226-2016$04.00/0

on the core size, the aggregation number, and the screening length.

Finally, section V summarizes the main results and contains some concluding remarks.

II. Theory

A rigorous theory of ionomeric colloids must describe many-body electrostatic and steric interactions between the colloidal aggregates, conformational equilibria of the ionomeric polymer chains, and solvent interactions. The complexity of the problem becomes apparent simply by enumerating the degrees of freedom; even in a simplified model, e.g., one where the solvent is treated as a continuum, the positions of the centers of mass of the colloidal aggregates, the positions of the monomers of the flexible ionomeric polymers, and the positions of the counterions must be considered. Henceforth, $\vec{R}_i$, $\vec{r}_{j,\alpha}^{(i)}$, and $\vec{r}_i$ denote the positions of the ith aggregate, the αth monomer unit on the jth ionomeric polymer attached to the ith aggregate measured relative to $\vec{R}_i$, and the ith counterion, respectively.

The configurational partition function for this system is given by

$$Z_c \equiv \int \prod_{i=1}^{N_c} d\vec{R}_i \prod_{j=1}^{N_A} \prod_{\alpha=1}^{N_m} d\vec{r}_{j,\alpha}^{(i)} \prod_{k=1}^{N_s} d\vec{r}_k \, e^{-\beta U} \tag{2.1}$$

where N_c, N_A, N_m, and N_s denote the number of colloidal aggregates, polymer chains per aggregate, the number of monomers per chain, and the number of salt ions, respectively, $\beta \equiv 1/k_B T$, and U is the potential energy. Equation 2.1 assumes that the system is monodisperse but can be trivially generalized at the expense of more complicated notation.

In this work, the average properties of a single chain will be considered, specifically, chain 1 on aggregate 1. To this end, the remaining degrees of freedom may be formally integrated out and the generating functional for single-chain properties becomes

$$Z_c^{(1)} \equiv \int \prod_{\alpha=1}^{N_m} d\vec{r}_{1,\alpha}^{(1)} \, e^{-\beta W} \tag{2.2}$$

where W is the potential of mean force for the specified chain. Similarly, the average of any single-chain property, denoted by A, becomes

$$\langle A \rangle = (Z_c^{(1)})^{-1} \int \prod_{\alpha=1}^{N_m} d\vec{r}_{1,\alpha}^{(1)} \, e^{-\beta W} A(\vec{r}_{1,1}^{(1)}, \ldots, \vec{r}_{1,N_m}^{(1)}) \tag{2.3}$$

where, henceforth, $\langle \ldots \rangle$ will denote a weighted average over single-chain configurations.

In general, the potential of mean force may be viewed as a functional of the average total monomer density, $\rho(\vec{r})$, and at present no exact expressions are available for it. In what follows, a phenomenological model for the single-chain potential of mean force will be developed.

Several important interactions must be considered when modeling W. The most obvious ones are those imposed by the impenetrability of the colloid core and by the connectivity of the ionomeric chain under consideration. The former will be described by an infinite spherical step potential at a core radius R_0, and this introduces an element of excluded volume into the problem. For the purposes of enumerating the allowed configurations which contribute to eq 2.2, the chain will be taken as ideal, although this last assumption can be relaxed.

In order to mathematically describe the configurational statistics of the chain, bond vectors, $\vec{\Delta}_\alpha \equiv \vec{r}_{\alpha,1}^{(1)} - \vec{r}_{\alpha-1,1}^{(1)}$, are introduced. For an ideal chain, contribution to the configurational probability density associated with the connectivity of the chain is given by

$$e^{-\beta W_c} \equiv \prod_{\alpha=1}^{N_m} w(\vec{\Delta}_\alpha | \vec{\Delta}_{\alpha-1}) \tag{2.4}$$

where w is the conditional bond probability density for having a specified bond vector given the preceding one. In the numerical work to be presented below, the chain will be modeled as freely jointed; hence,

$$w(\vec{\Delta}_\alpha | \vec{\Delta}_{\alpha-1}) = \chi(\Delta_\alpha) \equiv \frac{\delta(|\vec{\Delta}_\alpha| - a)}{4\pi a^2} \tag{2.5}$$

where a is the bond length and $\delta(x)$ is the Dirac δ-function.

Of course, real chains are not ideal, and, in particular, intra- and interchain excluded-volume effects should be considered. While this can be treated fairly rigorously for short or infinite single chains, here the ionomers around a single colloidal aggregate are not necessarily dilute, and, hence, interchain effects should also be considered on equal footing. Following Flory,[11,17] both effects will be treated by modeling the excluded-volume contribution to the potential of mean force as

$$\beta W_{ex} \equiv \nu \sum_{\alpha=1}^{N_m} \rho(\vec{r}_{1,\alpha}^{(1)}) \tag{2.6}$$

where ν is a phenomenological excluded-volume parameter and where $\rho(\vec{r})$ is the average total monomer number density (cf. eq 2.10). Since the ionomer density around a given colloidal aggregate is large, the intra- and inter-ionomer interactions are expected to be equally important; thus, it is probably not consistent to include the latter phenomenologically in eq 2.6 while treating the former exactly (e.g., by putting in the excluded-volume constraints when enumerating the conformations of a single chain), and, hence, eq 2.6 will be used to describe both effects. In addition, note that $\rho(r)$ also includes the monomer density associated with the specified chain and, hence, aspects of the intrachain excluded-volume effects of the specified chain.

Perhaps the most crucial of the possible interactions are electrostatic in nature. These include the intra- and interchain electrostatic interactions and the interactions with the ions in solution. These contributions to the potential of mean force, as a functional of the monomer density, can be calculated in several ways.

For dilute suspensions with sufficient screening between the colloidal aggregates, intercolloid interactions will be negligible. Hence, as long as the added salt concentration is not too high, the electrostatic contribution to the potential of mean force can be approximated by the mean electrostatic potentials, ϕ, at the monomer positions; i.e.,

$$W_{el} \equiv \sum_{\alpha=1}^{N_m} z_{m,\alpha}^{(1)} \phi(\vec{r}_{1,\alpha}^{(1)}) \tag{2.7}$$

where $z_{m,\alpha}^{(1)} \equiv z_m$ is the charge per monomer. Henceforth, they are assumed to be uniform and fully ionized. (Depending on the chemical nature of the ionic groups on the ionomers, this last assumption may not always be valid.)

Expressing the electrostatic contribution to the potential of mean force as the mean electrostatic potential is analogous to the approximation used in the Debye–Hückel theory of electrolyte solutions. In this work, the mean electrostatic potential will be determined from the lin-

earized Poisson–Boltzmann equation:

$$\nabla^2\phi = \kappa_D{}^2\phi - \frac{4\pi z_m}{\epsilon}\rho(\vec{r}) \tag{2.8}$$

where ϵ is the solvent dielectric constant, $\kappa_D \equiv \lambda_D{}^{-1} \equiv [4\pi\beta e^2 I/\epsilon]^{-1/2}$, λ_D is the Debye screening length, e is the charge of the electron, and I is the ionic strength of the ions in solution. Standard dielectric boundary conditions will be applied at the surface of the colloid.

The Green's function associated with eq 2.8 is easily computed for spherical colloid cores as an expansion in spherical harmonics and spherical Bessel functions.[18] Once this is done, noting that the average monomer density is spherically symmetric, it follows that

$$\phi(r) = \frac{2\pi z_m}{\kappa_D \epsilon r} \times \int_{R_0}^{\infty} dr' \left[e^{-\kappa_D|r-r'|} + \frac{(\kappa_D R_0 - 1)}{(\kappa_D R_0 + 1)} e^{-\kappa_D(r+r'-2R_0)} \right] r'\rho(r') \tag{2.9}$$

Note that the electric field inside the colloid core vanishes for spherically symmetric monomer distributions, and, hence, the dielectric constant of the core material does not appear in eq 2.9. As was argued for the excluded-volume contribution, the intrachain electrostatic interactions of the specified chain will not be considered explicitly.

The next step is to self-consistently determine the monomer density, and in this regard the approach is analogous to simple mean-field theories used to describe phase transitions (e.g., the Weiss mean-field theory of ferromagnetism). Specifically, the average monomer density must be computed using the distribution contained in eq 2.2; i.e.,

$$\rho(r) = N_A \langle \sum_{\alpha=1}^{N_m} \delta(\vec{r} - \vec{r}_{1,\alpha}^{(1)}) \rangle \tag{2.10}$$

In writing eq 2.10 it has been assumed that the places where the ionomer ends are attached to the colloid are randomly distributed over the core's surface.

The statistical mechanics of an ideal chain in an arbitrary external field cannot be solved in closed form. As is discussed in the appendix, for a given external potential, the chain can be viewed as a Markov process, and a hierarchy of integral equations can be derived for the conditional probability densities for the monomer positions. In the continuum limit, these equations can be approximated by coupled Fokker–Planck equations. In addition, the continuum equations can be solved analytically for neutral chains with no excluded volume.

In the current problem, the total monomer density must be computed and the effective potentials must be determined self-consistently. While this can be incorporated into the equations discussed in the appendix, getting any results will involve considerable numerical effort, even in the continuum limit. Moreover, as will be shown below, several interesting features of the model will be lost in the continuum limit. Instead of pursuing this approach, a Monte Carlo method will be used; this is now described.

III. Mean-Field Monte Carlo Method

If the potential of mean force appearing in eq 2.3 were known, it would then be a relatively simple matter to numerically evaluate the average by Monte Carlo sampling.[19,20] In the original method,[20] a sequence of configurations is generated, the energy of each configuration is computed, and the configuration is accepted with probability P, where

$$P \equiv \begin{cases} 1, & \text{if } \Delta E \le 0 \\ e^{-\beta\Delta E}, & \text{if } \Delta E > 0 \end{cases} \tag{3.1}$$

and where ΔE is the energy difference between the new and old configurations.

The way in which configurations are chosen to a large extent is arbitrary, with two important caveats. First, the choices must be reversible; specifically, the move from configuration $X \to X'$ must be as likely as $X' \to X$, whether or not the moves are actually accepted according to eq 3.1. The second restriction is that the chosen configurations, in principle, ultimately sample all configuration space.

Of course, there is still much freedom in choosing the moves. Ideally, they should be chosen to sample configuration space as rapidly as possible, although, in practice, this usually leads to an unacceptable number of moves being rejected. Several schemes have been constructed for chains in which the bond torsional angles take on continuous values. For example, there is the so-called *pivot* method[9,21] in which a bond is chosen at random, and the rest of the chain is randomly pivoted about that bond. Alternatively, there is the *displacement* method, in which a single bond is randomly displaced, keeping the bond length fixed (cf. eq 2.5), while the rest of the chain is simply translated.

Intuitively, it seems obvious that the pivot method should lead to a more rapid sampling of configurations. While this is indeed the case, when there are strong intrachain repulsions, it leads to an unacceptably large fraction of the moves being rejected. Of course, this problem can be reduced by decreasing the size of the rotation angles, although it turns out that the displacement method still seems to do better in this limit.

Since both methods require that random bond vectors (which, in the current model, have fixed length) be reversibly generated, polar coordinates, or Euler angles in the pivot method, will be used. These are chosen in the following manner:

$$\cos(\theta_{new}) = f(\cos(\theta_{old}) + 1 + \gamma_\theta \xi; 2) - 1 \tag{3.2a}$$

and

$$\phi_{new} = f(\phi_{old} + \gamma_\phi \xi; 2\pi) \tag{3.2b}$$

where θ and ϕ are the bond's polar and azimuthal angles, respectively, $\xi \in [-1/2, 1/2]$ is a uniformly generated random number

$$f(x;y) \equiv \begin{cases} x + y & \text{for } x < 0 \\ x - y & \text{for } x > y \\ x & \text{otherwise} \end{cases} \tag{3.3}$$

and where $\gamma_{\theta(\phi)} \le 1$ is used to adjust the size of the step in $\theta(\phi)$.

Of course, the usual Monte Carlo scheme assumes that the potentials are known, while here they must be determined self-consistently. Nonetheless, this is easily incorporated into the Monte Carlo evaluation of the averages. As usual, an initial chain configuration is chosen and is used (cf. eq 2.10) to compute an initial monomer density and effective potential. This potential[22] is then used in carrying out some Monte Carlo moves, after which the average monomer density and effective potentials are recalculated and the whole procedure is repeated until convergence is obtained.

As expected from eq 2.9, the mean electrostatic potential is relatively insensitive to the finer details of the density

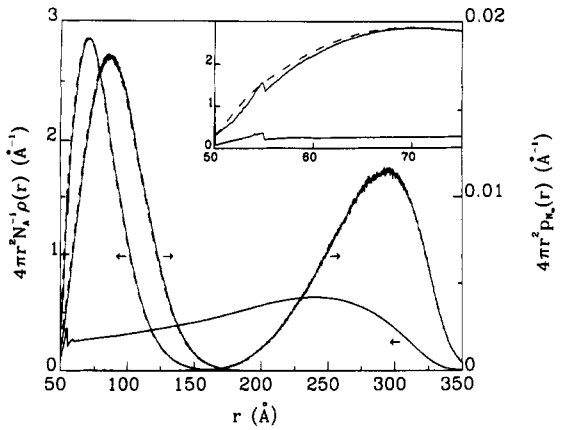

Figure 1. Total monomer density and end monomer probability density for uncharged chains near a core with R_0 = 50 Å and a = 5 Å. 10^7 Monte Carlo steps were used in obtaining the averages. The curves at shorter distances have no excluded volume, while those at longer distances had $\nu = (4/3)\pi a^3$ and N_A = 1000. The dashed curves are the results of the continuum calculation for neutral chains with no excluded volume described in the appendix (cf. eqs A.19 and A.21). Finally, the inset shows the total monomer density near the core.

profile, and, hence, it converges much more rapidly than the fluctuations in the Monte Carlo average decay.

IV. Results

Several examples have been considered using the method just described. Before examining cases where the ionomer was charged or had excluded volume, the method was tested on an uncharged random polymer next to a spherical core. Monte Carlo results are compared with the known continuum limit expressions described in the appendix for the total monomer density and the end monomer probability distribution in Figure 1.

As is well-known, the presence of the spherical core tends to exclude the polymer from the region of the core surface, although note that the monomer density is nonzero at the surface (cf. eqs A.11 and A.12). In general, the agreement between the continuum results and those of the simulation is very good, except on the scale of the monomer size. In particular, the discrete nature of the chain is reflected in the small jag in the total monomer density that occurs one bond length from the surface (cf. the inset).

Figure 1 also shows the effect of including excluded volume. As expected excluded-volume interactions lead to a swelling of the ionomer layer, the results here being similar to those obtained by others.[11,16] In addition, as in the other cases, the discrete nature of the chain is apparent only within a monomer distance from the core surface.

Some run parameters, run statistics, and the mean radius of gyration of the total chain and the end monomer are summarized in Table I. As the data in the table show, the chains swell with increasing excluded volume, aggregation number, or screening length. Excluded volume does not play a major role in the lesser screened systems; the electrostatic interactions are dominant, and, in any case, the local monomer density is smaller in the swollen state. The net charge in the ionomeric region, and hence the electrostatic repulsion, increases with the aggregation number. Finally note that the fluctuations in the end monomer position decrease as the chain swells. As will be seen more clearly below, this is due to an overall stiffening of the chain, which ultimately becomes an almost rigid rod.

The results presented in Table I do not tell the whole story. The total monomer density and the probability density for the end monomer unit are shown in Figures 2 and 3 for some of the cases listed in Table I. As expected, increasing the aggregation number, N_A, the screening length, or the excluded-volume parameter causes the ionomer to swell. While the swelling of the ionomer is already apparent from the data shown in Table I, notice the appearance of strongly localized monomers at the fully stretched monomer positions. The origin of these is easily understood in terms of the large repulsive electrostatic interactions and finite bond lengths. Clearly, these features would be absent in a continuum description but are seen in the molecular dynamics simulations of neutral chains by Murat and Grest.[16]

The monomer density near the core surface is shown in Figure 4. The stretched state of the chain in clearly apparent. In addition, note that the finite, rigid bond length leads to the asymmetric shape of the individual monomer peaks. A subtle effect associated with the excluded-volume interaction can be seen in Figure 4, where increasing the excluded-volume parameter, keeping everything else fixed, actually leads to a decrease in the order near the core surface.

This effect can be understood in terms of the simple Flory form for the excluded-volume interaction, where higher local density leads to increased repulsion. In a continuum model, this repulsion leads to further swelling of the chain; here, however, the finite-length, rigid bond does not allow this swelling to happen, and some of the monomers are pushed to shorter distances from the core. This smears out the local monomer density and reduces the excluded-volume interaction at the expense of increased electrostatic repulsion. This represents a kind of *frustration* which can be overcome by further reducing the screening. In addition, note that at larger distances, i.e., those where the chain is not fully stretched, the excluded-volume interaction leads to increased swelling, as might be expected naively.

The magnitude of this frustration effect is probably increased by the form of the excluded-volume interaction. In particular, the excluded-volume energy is local in the density. While this is reasonable on longer length scales, it surely must break down as the molecular scale is approached. Nonetheless, the effect should still be present, assuming that the ends of the monomers tend to avoid each other. A more correct expression would be nonlocal in the average monomer density, and this will be investigated in the future.

Finally, some mean potentials, i.e., both the electrostatic and excluded-volume contributions, are shown in Figure 5.

A close examination of the data in Figures 2–4 shows that the ionomeric region divides into roughly three subregions: (1) a fully stretched region near the core; (2) a flexible-rod-like region, where the fluctuations in monomer positions are comparable to the monomer size; and (3) an almost random polymer region where the fluctuations in the monomer positions are large. In the third region, the chain should resemble a random polymer, swollen by electrostatic repulsions, near the excluded-volume regions 1 and 2. This accounts for the "bump" in the total densities (cf. Figures 2 and 3).

The existence of a flexible-rod region can further be shown by examining the fluctuations in the individual monomer positions. This is done in Figure 6. Notice the rapid increase in the magnitude of the fluctuations at the bump positions. In addition, note that the fluctuations include the effects of rigid rotations of the rod around the point of attachement on the colloid core. It is easy to see that even small fluctuations in the orientation of a rod will be amplified by a factor of roughly $\langle r_i - R_0 \rangle$ when converting to position fluctuations.

Table I[a]

N_A	$(4/3)\pi a^3\nu$	λ_D (Å)	$\gamma_\phi = \gamma_\theta$	% moves rejected	$\langle\sum_{i=1}^{N_m} r_i^2\rangle^{1/2}/N_m^{-1/2}$ mean (Å)	SD[b] (Å)	$\langle r_{N_m}^2\rangle^{1/2}$ mean (Å)	SD[b] (Å)
10^2	0	1	1.0	9	108	28	132	24
10^2	0	5	0.75	22	167	52	217	27
10^2	0	10	0.5	29	230	80	310	35
10^2	0	10^2	0.5	76	366	156	562	12
10^2	0	10^3	0.25	87	386	171	626	4
10^2	1	1	0.5	14	149	45	191	29
10^2	1	5	0.75	24	177	56	230	27
10^2	1	10	0.5	29	232	81	313	35
10^2	1	10^2	0.5	76	366	156	561	12
10^2	1	10^3	0.25	87	386	171	626	4
10^3	0	1	0.25	7	146	43	185	29
10^3	0	5	0.75	35	226	74	297	33
10^3	0	10	0.25	35	305	116	426	33
10^3	0	10^2	0.25	90	388	172	632	4
10^3	0	10^3	0.25	98	391	174	647	1
10^3	1	1	0.25	16	214	73	285	35
10^3	1	5	0.75	40	242	84	324	35
10^3	1	10	0.25	35	306	117	428	34
10^3	1	10^2	0.25	90	387	172	631	4
10^3	1	10^3	0.01	66	390	174	647	1

[a] All cases have $R_0 = 50$ Å, $a = 5$ Å, $z_m = 1$ e, $N_m = 120$, $T = 298.15$ K, $\epsilon = 78.54$, and 10^7 configurations. [b] The SD columns contain the standard deviations of the total monomer and the end monomer probability distributions. Note that a fully stretched chain would have a radius of gyration of 391.2 (Å) and a standard deviation of 174.6 (Å) for the parameters used here.

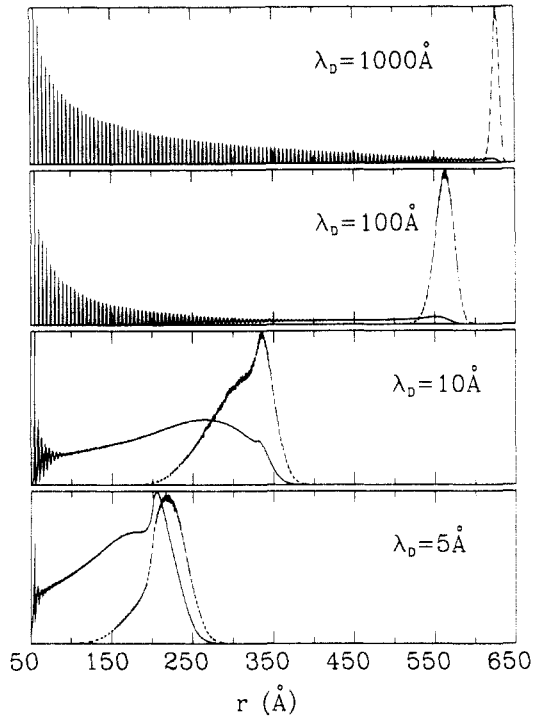

Figure 2. Monomer density and end probability density, $4\pi r^2\rho(r)$ (—) and $4\pi r^2 p_{N_m}(r)$ (- - -), for systems where $N_A = 100$ and $\nu = 0$. The remaining parameters are as in Table I. Each curve has been normalized such that its largest value is unity.

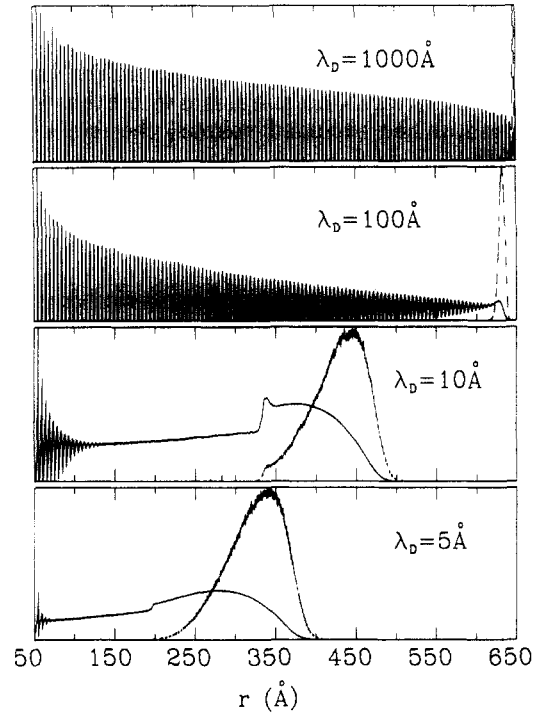

Figure 3. As in Figure 2, but now $N_A = 1000$ and $\nu = (4/3)\pi a^3$.

A crude estimate for the onset of the random-polymer region can be obtained as follows: If the ionomer becomes random at radius r, then the coil dimension will be $a[(R_{max} - r)/a]^{1/2}$, where R_{max} is the radius of the colloid when the ionomers are fully stretched. The mean distance between rodlike ionomers is $r(4\pi/N_A)^{1/2}$, and this must be sufficiently large such that the random-polymer ends of the ionomers are separated by one or more Debye screening lengths. If not, interchain electrostatic or steric repulsion will lead to further swelling. Hence, random-polymer behavior should be observed when

$$a[(R_{max} - r)/a]^{1/2} + \alpha\lambda_D = r(4\pi/N_A)^{1/2} \qquad (4.1)$$

where $\alpha \sim O(1)$.[23] This equation is easily solved for r, and the result qualitatively explains the trends shown in Figures 2 and 3.

Thus, for poorly screened ionomers, the region near the colloid core should be highly ordered while that near the ionomer outer surface should still be liquidlike. As the screening is increased by adding additional salt, the ordered region gradually *melts* and condenses around the core. Note that the curvature of the core plays an essential role in these transitions, since moving to longer radii allows the ionomer density to decrease; different behavior should be observed near flat surfaces with a fixed *surface density* of ionomers.

The change in the degree of local order will be accompanied by large changes in the colloid form factors as measured in scattering experiments. If the scattering amplitudes of all the monomers are assumed to be equal and that scattering from the colloid core can be ignored

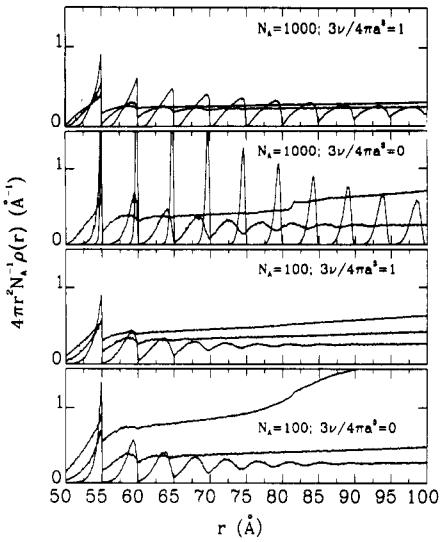

Figure 4. Variation of the total monomer densities near the colloid core with increasing screening length. Each panel shows results for λ_D = 1, 5, and 10 Å (with increasing degrees of order). The other parameters are given in Table I.

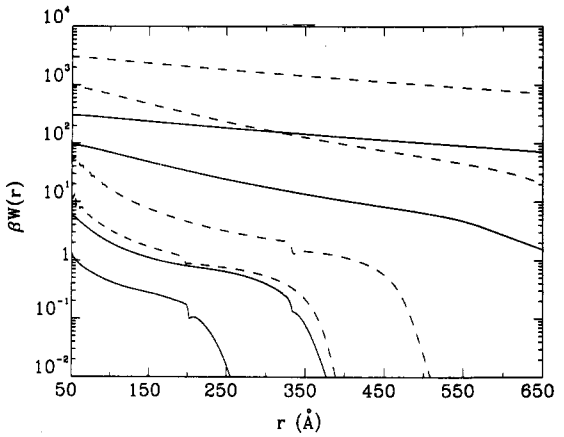

Figure 5. Mean potentials for the cases presented in Figures 2 (solid) and 3 (dashed). Note that both the electrostatic and excluded-volume contributions are included (dashed).

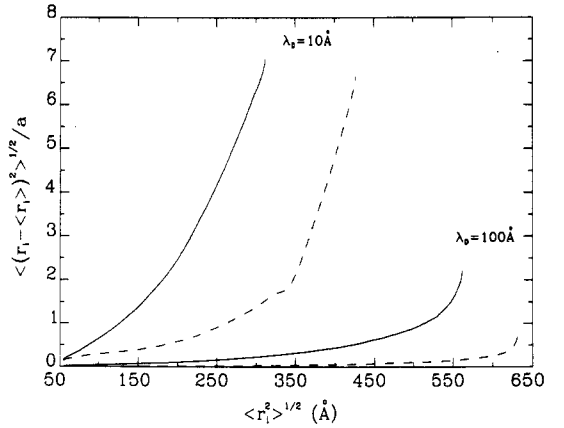

Figure 6. Standard deviation of the monomer radii (in units of the bond length) as a function of the average monomer positions. The solid and dashed curves have N_A = 100 and 1000, respectively, while λ_D = 10 and 100 Å had $\nu = (4/5)\pi a^3$ and 0, respectively.

(or corrected for), it then follows that the form factor will be proportional to the Fourier transform of the total monomer density; i.e.,

$$S(q) \propto \left|\frac{4\pi}{q}\int_{R_0}^{\infty} dr\, r \sin(qr)\, \rho(r)\right|^2 \qquad (4.2)$$

where q is the scattering wavevector in the experiment. The integral on the right-hand side of eq 4.2 has been

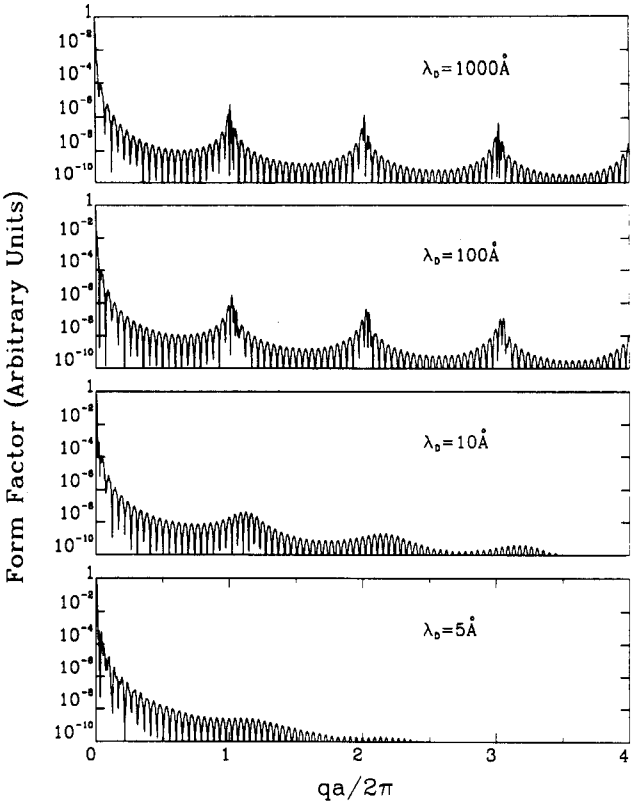

Figure 7. Form factors for the cases shown in Figure 2.

computed numerically, and the results are shown in Figure 7.

As expected, as the chains become more rodlike, peaks build up where the Bragg condition, $qa = 2n\pi$, is satisfied. (For real ionomers, the Bragg condition will have to be modified in order to account for the molecular structure of the monomers.) In addition to these features there are smaller oscillations arising from the Fourier transform of a nonuniform shell, where the periods of the oscillations are in the range π/R_0 and $\pi/(R_0 + \Delta)$, where Δ is a measure of the thickness of the ionomeric layer.

V. Discussion

In this work, a simple method for treating the equilibrium properties of strongly interacting ionomeric chains attached to a colloidal core has been presented. Since much of the calculation was based on a mean-field approximation for many of the interactions and only numerically treats the properties of a single ideal chain, the numerical effort in obtaining results was trivial and can easily be applied to much longer chains.

The present calculation has been simplified in several respects. First, the interaction with counterions has been treated within the linearized Debye–Hückel approximation. It is not obvious whether this is valid inside the ionomeric region, where electrostatic potential and counterion concentration can be large, and in the light of the detailed calculations of Valleau on polyelectrolytes.[9] Nonetheless, given the rapid convergence of the mean electrostatic potentials, it is entirely feasible to go beyond this approximation, and results along these lines will be presented in the near future.

A second simplification has been to omit the intrachain–single-chain electrostatic and excluded-volume interactions. As was argued in section II, this is a reasonable approximation when the local ionomer density is large but will break down for a sufficiently low local density. While there is no reason why these interactions cannot be explicitly included in principle, the numerical effort

required will be considerable.[9] Needless to say, it is probable that the intrachain–single-chain interactions will only lead to further swelling (and, ultimately, more rodlike character) of the chain.

Finally, the colloid core has been assumed to be completely rigid, and, hence, the ionomers are permanently anchored, irrespective of the electrostatic repulsions between chains. This is reasonable for temperatures below the glass transition temperature, although it will break down as the temperature is raised. Indeed, in extreme situations, it is conceivable that the block-copolymer aggregate could break apart as the screening is reduced.

The main conclusion of this work is that there is not a single morphology which describes the ionomeric layer around a colloidal aggregate. As has been shown, the ionomeric region can roughly be divided into three subregions: a rigid rodlike region near the colloid core, followed by a flexible-rod region, and finally, a continuum random-polymer region. The extent of these regions is controlled by the screening length, by the charge per ionomer, and by the aggregation number. (The latter helps determine the local charge density, which in turn, affects the electrostatic repulsion.) In addition, while the overall swelling of the ionomers will be found in continuum theories, many of the features found here will be absent, in particular, those having to do with rigid-rod behavior or with excluded-volume frustration.

Acknowledgment. I thank Adi Eisenberg, Bruce Lennox, and John Valleau for useful discussions. A portion of this work was supported by the National Sciences and Engineering Research Council of Canada and by Le Fonds pour la Formation de Chercheurs et l'Aide à la Recherche du Québec.

Appendix: Ideal Chains in External Fields

In this appendix, the potential is assumed to be known and an exact hierarchy of integral equations giving the conditional probabilities of finding any monomer in the chain at any given position, given that the preceding one is at some specified point, is presented and discussed in the continuum limit. Let $p_n(\vec{r}_n,\vec{r}_{n-1},...,\vec{r}_1)$ be the joint probability density for having monomer 1 at $\vec{r}_1$, monomer 2 at $\vec{r}_2$, etc. From eq 2.2 it follows that

$$p_n(\vec{r}_n,...,\vec{r}_1) = \int d\vec{r}_{n+1}...d\vec{r}_{N_m} \frac{\prod_{i=1}^{N_m}\{\chi(\vec{r}_i-\vec{r}_{i-1})e^{-\beta W(\vec{r}_i)}\}}{Z_c^{(1)}} \quad (A.1)$$

where the parts of W describing the connectivity of the chain (cf. eqs 2.4 and 2.5) have been explicitly written out. It is well-known that ideal chains are Markov. Conditional probability densities are introduced as

$$\Omega_n(r_n|r_{n-1},...,r_1) \equiv \frac{p_n(\vec{r}_n,...,\vec{r}_1)}{p_{n-1}(\vec{r}_{n-1},...,\vec{r}_1)} = \frac{\chi(\vec{r}_n-\vec{r}_{n-1})e^{-\beta W(\vec{r}_n)}x_n(\vec{r}_n)}{x_{n-1}(\vec{r}_{n-1})} \quad (A.2)$$

where

$$x_n(\vec{r}_n) \equiv \int d\vec{r}_{n+1}...d\vec{r}_{N_m}\prod_{i=n+1}^{N_m}\{\chi(\vec{r}_i-\vec{r}_{i-1})e^{-\beta W(\vec{r}_i)}\} \quad (A.3)$$

Roughly speaking, $x_n(\vec{r})$ is a measure of the number of configurations the remaining monomers of the chain can adopt given that monomer n is at $\vec{r}$. Hence, in a system with a surface, $x_n(\vec{r})$ should be smaller near the surface, *even in the absence of any other interactions.*[10,11]

The conditional probabilities only depend on the preceding monomer position; hence, the chain is Markov. However, note that the chain does not correspond to a simple random walk in an external field (i.e., the x's on the right-hand side of eq A.2 are not constant).

From the definition of x_n, it follows that

$$x_n(\vec{r}_n) \equiv \int d\vec{r}_{n+1}\chi(\vec{r}_{n+1}-\vec{r}_n)e^{-\beta W(\vec{r}_{n+1})}\chi_{n+1}(\vec{r}_{n+1}) \quad (A.4)$$

for $n < N_m$, with

$$x_{N_m}(\vec{r}) \equiv 1 \quad (A.5)$$

Once this hierarchy of integral equations is solved, the conditional probabilities are easily constructed using eq A.2, and from these any average property of the chain can be computed using the standard properties of Markov processes. For example, if $p_n(\vec{r})$ is the probability density that the nth monomer is at $\vec{r}$, it follows that

$$p_n(\vec{r}) = \int d\vec{r}'\,\Omega_n(\vec{r}|\vec{r}')\,p_{n-1}(\vec{r}') = \int d\vec{r}'\,\chi(\vec{r}-\vec{r}')\,e^{-\beta W(\vec{r})}x_n(\vec{r})\frac{p_{n-1}(\vec{r}')}{x_{n-1}(\vec{r}')} \quad (A.6)$$

where $\Omega_n(\vec{r}|\vec{r}')$ is given by eq A.2.

In order to see how $x_n(r)$ modifies the monomer probabilites and densities, consider the continuum limits of eqs A.3 and A.6 (i.e., $a \to 0$ keeping na^2 constant) for a neutral chain, with no excluded volume, near a spherical core. The well-known Kramers–Moyal expansion[23] is used and gives

$$-\frac{\partial x_n(\vec{r})}{\partial n} = [e^{-\beta W(\vec{r})}-1]x_n(\vec{r}) + \frac{a^2}{6}\nabla^2[e^{-\beta W(\vec{r})}x_n(\vec{r})] \quad (A.7)$$

and

$$\frac{\partial q_n(\vec{r})}{\partial n} = [e^{-\beta W(\vec{r})}-1]q_n(\vec{r}) + \frac{a^2e^{-\beta W}(\vec{r})}{6}\nabla^2 q_n(\vec{r}) \quad (A.8)$$

where $q_n(\vec{r}) \equiv p_n(\vec{r})/x_n(\vec{r})$. The initial condition in n for $x_n(\vec{r})$ is given by eq A.5, while, for chains that are uniformly distributed on the core,

$$q_0(\vec{r}') = \frac{\delta(r-R_0)}{4\pi R_0^2 x_0(R_0)} \quad (A.9)$$

The boundary conditions at the core are more subtle. From eqs A.4 and 2.5 it follows that

$$R_0x_n(R_0) = \frac{1}{2a}\int_{R_0}^{R_0+a} d\xi\,\xi x_{n+1}(\xi)\,e^{-\beta W(\xi)} \quad (A.10)$$

where spherical symmetry has been assumed and where only the slowly varying parts of W should be included in the integrand. Since the integrand is expected to vary smoothly, $x_{n+1}(\xi)$ can be expanded in a Taylor series around $\xi = R_0$. Similarly, $x_n(R_0)\,e^{-\beta W(\xi)}$ can be expanded around $n = n+1$, and the n derivatives evaluated by using eq A.7. If terms containing two or more derivatives in r are

dropped, this gives

$$L\frac{\partial e^{-\beta W(r)}x_n(r)}{\partial r} = e^{-\beta W(r)}x_n(r) \qquad \text{(A.11)}$$

at $r = R_0$, where

$$L \equiv \frac{a(3R_0 - 2a)}{3(2R_0 - a)} \sim \frac{a}{2}, \quad \text{for } R_0 \gg a \qquad \text{(A.12)}$$

The boundary condition for the auxiliary function $q_n(r)$ now follows from the requirement that

$$\frac{\mathrm{d}}{\mathrm{d}n}\int \mathrm{d}\vec{r}\, p_n(\vec{r}) = 0 \qquad \text{(A.13)}$$

It is easy to show that eq A.13 will hold if $q_n(r)$ obeys the same boundary conditions as $e^{-\beta W(r)}x_n(r)$; i.e.,

$$L\frac{\partial q_n(r)}{\partial r} = q_n(r) \qquad \text{(A.14)}$$

Equations A.7 and A.8 and their boundary conditions (cf. eqs A.11 and A.14) are very similar; indeed, once the Green's function for either of them is known, the problem is in effect solved. In order to show this, a retarded Green's function, $G_n(\vec{r}|\vec{r}')$, is defined by

$$\frac{\partial G_n(\vec{r}|\vec{r}')}{\partial n} = [e^{-\beta W(\vec{r})} - 1]G_n(\vec{r}|\vec{r}') + \frac{a^2 e^{-\beta W(\vec{r})}}{6}\nabla^2 G_n(\vec{r}|\vec{r}') + \delta(\vec{r}-\vec{r}')\,\delta(n) \qquad \text{(A.15)}$$

where $G_n(\vec{r}|\vec{r}')$ satisfies the boundary condition given in eq A.14. It is easy to express both x_n and q_n as integrals of G; in particular,

$$q_n(\vec{r}) = \int \mathrm{d}\vec{r}'\, G_n(\vec{r}|\vec{r}')\, q_0(\vec{r}') \qquad \text{(A.16)}$$

and

$$x_n(\vec{r}) = \int \mathrm{d}\vec{r}'\, G_{N_m-n}(\vec{r}|\vec{r}')\, e^{-\beta[W(\vec{r}')-W(\vec{r})]} \qquad \text{(A.17)}$$

For problems with spherical symmetry, G can be represented by a sum of products of spherical harmonics, and, for the initial conditions given by eqs A.5 and A.9, only the $l = 0$ term will contribute to eqs A.16 and A.17. If the radial factor for the $l = 0$ term is denoted as $g_n(r|r')$ and is used in eqs A.16 and A.17, it follows that

$$p_n(r) = \frac{g_n(r|R_0)\int \mathrm{d}r'\, r'^2 g_{N_m-n}(r|r')\, e^{-\beta[W(r')-W(r)]}}{4\pi\int \mathrm{d}r'\, r'^2 g_{N_m}(R_0|r')\, e^{-\beta[W(r')-W(R_0)]}} \qquad \text{(A.18)}$$

With the exception of the explicit $e^{-\beta W}$ factors, this last result is identical with the expressions found in refs 10 and 11. The additional factors arise from those in the diffusion terms in eqs A.7 and A.9. These equations differ from those in refs 10 and 11 in two other ways: First, the potential has not been assumed to be small, and, hence, the factors of $e^{-\beta W(\vec{r})} - 1$ have not been approximated as $-\beta W(\vec{r})$ in the first terms on the right-hand sides of eqs A.7 and A.8. The second difference is in the boundary condition. The $a \to 0$ limit has not been strictly enforced in deriving the boundary condition; if it was, then, as is discussed in ref 11b, there is some ambiguity in taking the $r' \to R_0$ limit in eq A.18.

Finally, note that Eqs A.7–A.14 can be solved analytically using Laplace transforms when $W(r) = 0$. The result is

$$x_n(r) = 1 + \frac{R_0^2}{r(R_0+L)}\left[\exp\left(\frac{(R_0+L)(r-R_0)}{LR_0} + \frac{(R_0+L)^2a^2(N_m-n)}{6R_0^2L^2}\right)\mathrm{erfc}\left(\frac{(R_0+L)a(N_m-n)^{1/2}}{6^{1/2}LR_0} + \frac{(r-R_0)6^{1/2}}{2a(N_m-n)^{1/2}}\right) - \mathrm{erfc}\left(\frac{(r-R_0)6^{1/2}}{2a(N_m-n)^{1/2}}\right)\right] \qquad \text{(A.19)}$$

and

$$p_n(r) = \frac{x_n(r)}{4\pi r R_0 a x_0(R_0)}\left[\left(\frac{6}{\pi n}\right)^{1/2}\exp\left(-\frac{3(r-R_0)^2}{2na^2}\right) - \frac{(R_0+L)a}{LR_0}\exp\left(\frac{(R_0+L)(r-R_0)}{LR_0} + \frac{(R_0+L)^2na^2}{6L^2R_0^2}\right)\times \mathrm{erfc}\left(\frac{(R_0+L)an^{1/2}}{6^{1/2}LR_0} + \frac{(r-R_0)6^{1/2}}{2an^{1/2}}\right)\right] \qquad \text{(A.20)}$$

where $\mathrm{erfc}(x)$ is the complimentary error function.

In general, $x_n(r)$ is not constant and, hence, modifies the monomer probabilities from what would be obtained by modeling the chain as a simple random walk near a specularly reflecting boundary. For the sake of comparison, the monomer probability densities in this problem are

$$p_{n,\mathrm{random}}(r) = \frac{1}{4\pi r R_0}\left[\left(\frac{6}{\pi n a^2}\right)^{1/2}\exp\left(-\frac{3(r-R_0)^2}{2na^2}\right) - R_0^{-1}\exp\left(\frac{(r-R_0)}{R_0} + \frac{na^2}{6R_0^2}\right)\mathrm{erfc}\left(\frac{an^{1/2}}{6^{1/2}R_0} + \frac{(r-R_0)6^{1/2}}{2an^{1/2}}\right)\right] \qquad \text{(A.21)}$$

References and Notes

(1) Schaefer, D. W.; Berne, B. J. *Phys. Rev. Lett.* **1974**, *32*, 1110. Schaefer, D. W. *J. Chem. Phys.* **1977**, *66*, 3980. Schaefer, D. W.; Ackerson, B. J. *Phys. Rev. Lett.* **1975**, *35*, 1448. Williams, R.; Crandell, R. S.; Wojtowitz, P. J. *Phys. Rev. Lett.* **1976**, *37*, 348. Clark, N. A.; Hurd, A. J.; Ackerson, B. J. *Nature* **1979**, *281*, 58. For a review, see, e.g.: Pieranski, P. *Contemp. Phys.* **1983**, *24*, 25.

(2) Verwey, E. J. W.; Overbeek, J. Th. G. *Theory of the Stability of Lyophobic Colloids*; Elsevier: New York, 1948.

(3) See, e.g.: Khan, S.; Morton, T.; Ronis, D. *Phys. Rev. A.* **1987**, *35*, 4295.

(4) Sheu, E. Y.; Wu, C.-F.; Chen, S.-H.; Blum, L. *Phys. Rev. A* **1985**, *32*, 3807. Chen, S.-H. *Physics of Amphiphiles: Micelles, Vesicles and Microemulsions*; 1985; p 281. Chao, Y.-S.; Sheu, E. Y.; Chen, S.-H. *J. Phys. Chem.* **1985**, *89*, 4862. Bratko, D.; Friedman, H. L.; Chen, S.-H.; Blum, L. *Phys. Rev.* **1986**, *A34*, 2215.

(5) Zhu, J.; Lennox, R. B.; Eisenberg, A. *J. Am. Chem. Soc.* **1991**, *113*, 5583; *Langmuir* **1991**, *7*, 1579.

(6) Ronis, D. *Phys. Rev. A* **1991**, *44*, 3769.

(7) See, e.g.: Hill, T. L. *Introduction to Statistical Thermodynamics*; Addison-Wesley: Reading, MA, 1960; Chapter 21.

(8) For some recent examples on polyampholytes, see, e.g.: Higgs, P. G.; Joanny, J.-F. *J. Chem. Phys.* **1991**, *94*, 1543. Kantor, Y.; Kardar, M. *Europhys. Lett.* **1991**, *14*, 421. Kantor, Y.; Li, H.; Kardar, M. *Phys. Rev. Lett.* **1992**, *69*, 61.

(9) Valleau, J. P. *Chem. Phys.* **1989**, *129*, 163.

(10) Di Marzio, E. A. *J. Chem. Phys.* **1965**, *42*, 2101.

(11) (a) Edwards, S. F. *Proc. Phys. Soc.* **1965**, *85*, 613. (b) Dolan, A. K.; Edwards, S. F. *Proc. R. Soc.* **1975**, *A343*, 427.

(12) Dan, N.; Tirrell, M. *Macromolecules* **1992**, *25*, 2890.

(13) Dolan, A. K.; Edwards, S. F. *Proc. R. Soc.* **1974**, *A337*, 509.

(14) See, e.g.: Alexander, S. *J. Phys. (Paris)* **1976**, *38*, 977. de Gennes, P.-G. *Scaling Concepts in Polymer Physics*; Cornell University Press: Ithaca, NY, 1979. Witten, T. A.; Pincus, P. A. *Macromolecules* **1986**, *19*, 2509.

(15) Ball, R. C.; Marko, J. F.; Milner, S. T.; Witten, T. A. *Macromolecules* **1991**, *24*, 693.

(16) Grest, G.; Kremer, K.; Witten, T. A. *Macromolecules* **1987**, *20*,

1376. Murat, M.; Grest, G. *Macromolecules* **1991**, *24*, 704.
(17) Flory, P. *Principles of Polymer Chemistry*; Cornell University Press: Ithaca, NY, 1971; Chapter XII.
(18) See, e.g.: Morris, P. M.; Feshbach, H. *Methods of Theoretical Physics*; McGraw-Hill Book Co.: New York 1953.
(19) See, e.g.: Valleau, J. P.; Whittington, S. G.; or Valleau, J. P.; Torrie, G. In *Statistical Mechanics Part A: Equilibrium Techniques*; Berne, B. J., Ed.; Plenum Press: New York, 1977; Chapters 4 and 5.
(20) Metropolis, N.; Metropolis, A. W.; Rosenbluth, M. N.; Teller, A. H.; Teller, E. *J. Chem. Phys.* **1953**, *21*, 1087.
(21) For a discussion of the pivot algorithm on lattices, see, e.g.: Lal, M. *Mol. Phys.* **1969**, *17*, 57. Madras, N.; Sokall, A. D. *J. Stat. Phys.* **1988**, *50*, 109. For a discussion of egrodicity and the choice of Monte Carlo steps, also see: Madras, N.; Sokall, A. D. *J. Stat. Phys.* **1987**, *47*, 573.
(22) In actual practice, the potential turns out to be relatively smooth; hence, in the numerical work, it is evaluated at a uniformly spaced grid of points and cubic splines are used to calculate the potential intermediate points.
(23) In writing this last equation, it has been assumed that the key electrostatic length scale is the Debye screening length and not, for example, the Beijrum length. The latter could be more important in weakly charged systems.
(24) See, e.g.: Chandrasekhar, S. *Rev. Mod. Phys.* **1943**, *15*, section 4, 1.